

# Current Biology

## Probabilistic Models of Larval Zebrafish Behavior Reveal Structure on Many Scales

### Highlights

- Naturalistic larval zebrafish behavior is observed with a moving camera system
- Probabilistic models are used to predict and simulate behavioral sequences
- Models combine environmental dynamics, behavioral history, and hunger state
- Simulations capture behavioral dynamics spanning multiple timescales

### Authors

Robert Evan Johnson,  
Scott Linderman, Thomas Panier, ...,  
Kristian Joseph Herrera, Andrew Miller,  
Florian Engert

### Correspondence

robertevanjohnson@gmail.com

### In Brief

Johnson et al. use a moving camera system to observe naturalistic larval zebrafish behavior and develop probabilistic models to predict and simulate behavioral sequences. Their simulations capture behavioral dynamics spanning multiple timescales, from reactions to prey to hunger-dependent changes in action selection across hunting and exploration.



# Probabilistic Models of Larval Zebrafish Behavior Reveal Structure on Many Scales

Robert Evan Johnson,<sup>1,2,8,9,\*</sup> Scott Linderman,<sup>3,4,8</sup> Thomas Panier,<sup>1,5</sup> Caroline Lei Wee,<sup>1,2,6</sup> Erin Song,<sup>1</sup> Kristian Joseph Herrera,<sup>1</sup> Andrew Miller,<sup>7</sup> and Florian Engert<sup>1</sup>

<sup>1</sup>Department of Molecular and Cellular Biology, Harvard University, 16 Divinity Avenue, Cambridge, MA 02138, USA

<sup>2</sup>Graduate Program in Neuroscience, Harvard University, 220 Longwood Avenue, Boston, MA 02115, USA

<sup>3</sup>Department of Statistics, Stanford University, 390 Serra Mall, Stanford, CA 94305, USA

<sup>4</sup>Wu Tsai Neurosciences Institute, Stanford University, 318 Campus Drive, Stanford, CA 94305, USA

<sup>5</sup>Sorbonne Université, CNRS, Institut de Biologie Paris-Seine, Laboratoire Jean Perrin, 4 Place Jussieu, 75005 Paris, France

<sup>6</sup>Institute of Molecular and Cell Biology, A\*STAR, 61 Biopolis Drive, 138673 Singapore, Singapore

<sup>7</sup>Data Science Institute, Columbia University, 550 W 120th Street, New York City, NY 10027, USA

<sup>8</sup>These authors contributed equally

<sup>9</sup>Lead Contact

\*Correspondence: [robertevanjohnson@gmail.com](mailto:robertevanjohnson@gmail.com)

<https://doi.org/10.1016/j.cub.2019.11.026>

## SUMMARY

Nervous systems have evolved to combine environmental information with internal state to select and generate adaptive behavioral sequences. To better understand these computations and their implementation in neural circuits, natural behavior must be carefully measured and quantified. Here, we collect high spatial resolution video of single zebrafish larvae swimming in a naturalistic environment and develop models of their action selection across exploration and hunting. Zebrafish larvae swim in punctuated bouts separated by longer periods of rest called interbout intervals. We take advantage of this structure by categorizing bouts into discrete types and representing their behavior as labeled sequences of bout types emitted over time. We then construct probabilistic models—specifically, marked renewal processes—to evaluate how bout types and interbout intervals are selected by the fish as a function of its internal hunger state, behavioral history, and the locations and properties of nearby prey. Finally, we evaluate the models by their predictive likelihood and their ability to generate realistic trajectories of virtual fish swimming through simulated environments. Our simulations capture multiple timescales of structure in larval zebrafish behavior and expose many ways in which hunger state influences their action selection to promote food seeking during hunger and safety during satiety.

## INTRODUCTION

Methods to quantify freely moving animal behavior are quickly advancing as cameras, pose estimation algorithms, and behavioral models improve. Modern behavioral analysis pipelines [1] commonly involve (1) acquiring behavioral video, (2) extracting

low-dimensional time series representations of postural dynamics, and (3) annotating each image frame with a behavioral state label (e.g., “head-grooming” and “rearing”). Variations of this pipeline have been used to discover sets of stereotyped actions generated by worms [2–5], flies [6–8], fish [9–13], and mice [14]. Importantly, these methods produce statistical behavioral summaries to facilitate comparison of nervous system function across animals.

Larval zebrafish are convenient to use in behavioral studies due to their simple body plan, temporally discrete behavior, and stereotyped locomotor repertoire. With their compact shape and limited flexibility, automatic posture tracking [15–17] of larval zebrafish is uncomplicated. Since larvae swim in punctuated bouts, temporal segmentation of their behavior into bout and interbout epochs is also straightforward. Together, the anatomy and movement of zebrafish larvae simplify behavioral analyses, allowing swim bouts to be represented as points in a high-dimensional posture or kinematic parameter space. Several studies have leveraged these properties to categorize swim bouts. The most comprehensive effort [13] identified 13 basic types used during hunting [18, 19], taxis behaviors [20–23], escape maneuvers [24–26], social interactions [27], and spontaneous swimming in light and dark.

While larval zebrafish locomotor patterns have been well studied, much less is known about the complex generative processes underlying their natural behavioral sequences. How do external inputs (e.g., prey positions and properties) and internal inputs (e.g., behavioral history and hunger state) combine to influence action selection? To address this general problem, we use a moving camera system to collect high spatial resolution video of individual larvae swimming in a large arena with abundant prey. This approach eliminates a rigid trade-off between spatial resolution and arena size, allowing us to observe hundreds of consecutive swim bouts without interference from arena boundaries. We then use these data to construct probabilistic behavioral models—building on point process models with a long history in computational neuroscience [28–31]—to evaluate how internal and external inputs shape behavior. By sampling from these models, we simulate larval trajectories capturing behavioral dynamics spanning multiple timescales,



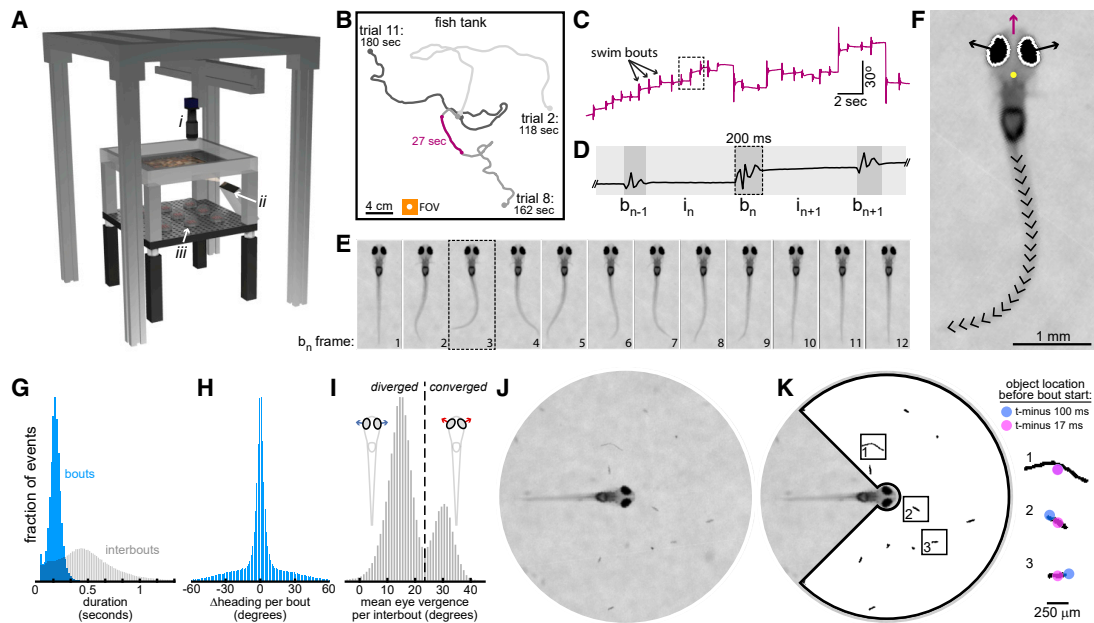


**Figure 1. Acquiring Behavioral Data with BEAST**

- (A) BEAST schematic. Infrared camera (i) moves on motorized gantry to stay above fish. Frame rate = 60 fps. Projector (ii) and IR-LEDs (iii) illuminate screen embedded in tank bottom. See [Video S1](#) for animated schematic.
- (B) Swim paths from three trials from one fish. Arena water volume = 300 × 300 × 4 mm. Camera field of view = 22 × 22 mm (orange square).
- (C) Fish heading direction over time (from purple section in B).
- (D) Expansion of box from (C) with bout and interbout epochs identified (notation indicated).
- (E) One swim bout (from box in D) after image registration.
- (F) Head position (yellow dot), heading direction (purple arrow), eye vergence angles (angles of black arrows above horizontal), and tail shape (20 tail tangent directions) extracted in every frame (frame 3 from E shown). See [Figure S1](#) for details.
- (G) Histograms of all bout and interbout durations.
- (H) Histogram of heading direction change per bout ( $\Delta$ heading).
- (I) Histogram of mean eye vergence per interbout. Convergence threshold set at local minimum: 24°.
- (J) Video dataset cropped to circular FOV (diameter = 8.12 mm).
- (K) Locations, sizes, shapes, and relative velocities of putative prey are identified preceding initiation of every swim bout (here shown for objects in J). Box width = 820  $\mu$ m. Identified objects are mostly edible (paramecia, rotifers), but include also algae, dust (box 1), and artifacts.

from reactions to prey (<100 ms), across stretches of hunting and exploration (seconds to minutes), and throughout changing hunger state (minutes to hours).

## RESULTS

### Acquiring Behavioral Data with BEAST

We constructed BEAST (behavioral evaluation across space-time; [Figure 1A](#); [Video S1](#)) to observe 7- to 8-day-post-fertilization *nacre* zebrafish larvae ( $n = 130$ ) one at a time. To evaluate how hunger influences behavior, each fish was given abundant paramecia (fed group,  $n = 73$ ) or deprived of food for 2.5–5 h (starved group,  $n = 57$ ) prior to observation. Previous studies show that brief food deprivation robustly increases larval zebrafish food intake [[32](#), [33](#)] and that hunger increases their likelihood to approach, rather than avoid, prey-like visual stimuli [[34](#), [35](#)]. We therefore expect our fed and starved fish groups to display different behavioral patterns and aim to construct models to quantify these effects.

We place each fish in the arena and repeatedly recruit it to the center to initiate up to 18 observational trials. We leverage the optomotor response [[23](#)] to guide fish to the center by projecting

optic flow stimuli onto a screen embedded in the tank bottom. Once at the center, a static natural scene replaces the gratings and the fish is recorded for up to 3 min or until it reaches the arena edge or tracking fails. Swim paths from three representative trials are shown ([Figure 1B](#)) and the fish's heading direction throughout a portion of one trial is plotted ([Figure 1C](#)). Swim bouts are seen as brief fluctuations in heading direction over time, and the timing of bout and interbout epochs is determined from this signal ([Figure 1D](#)). We translate and rotate each image frame to register the video to the fish's reference frame ([Figure 1E](#)) and encode fish posture by estimating eye vergence angles [[19](#)] and tail shape [[36](#)] ([Figures 1F](#) and [S1](#)). Larvae can accelerate rapidly (e.g., during escape swims), sometimes causing online tracking failure. Offline pose estimation is also occasionally compromised due to motion blur (during very high-speed swims) or body roll (causing one eye to occlude the other in the image). We retain only video segments in which all postural features are accurately extracted in every frame for further analysis.

The processed dataset contains 40 h of behavioral data (4,002 video segments) parsed into bout and interbout epochs ([Figure 1G](#)). Across all swim bouts ( $n = 200,559$ ), heading angle

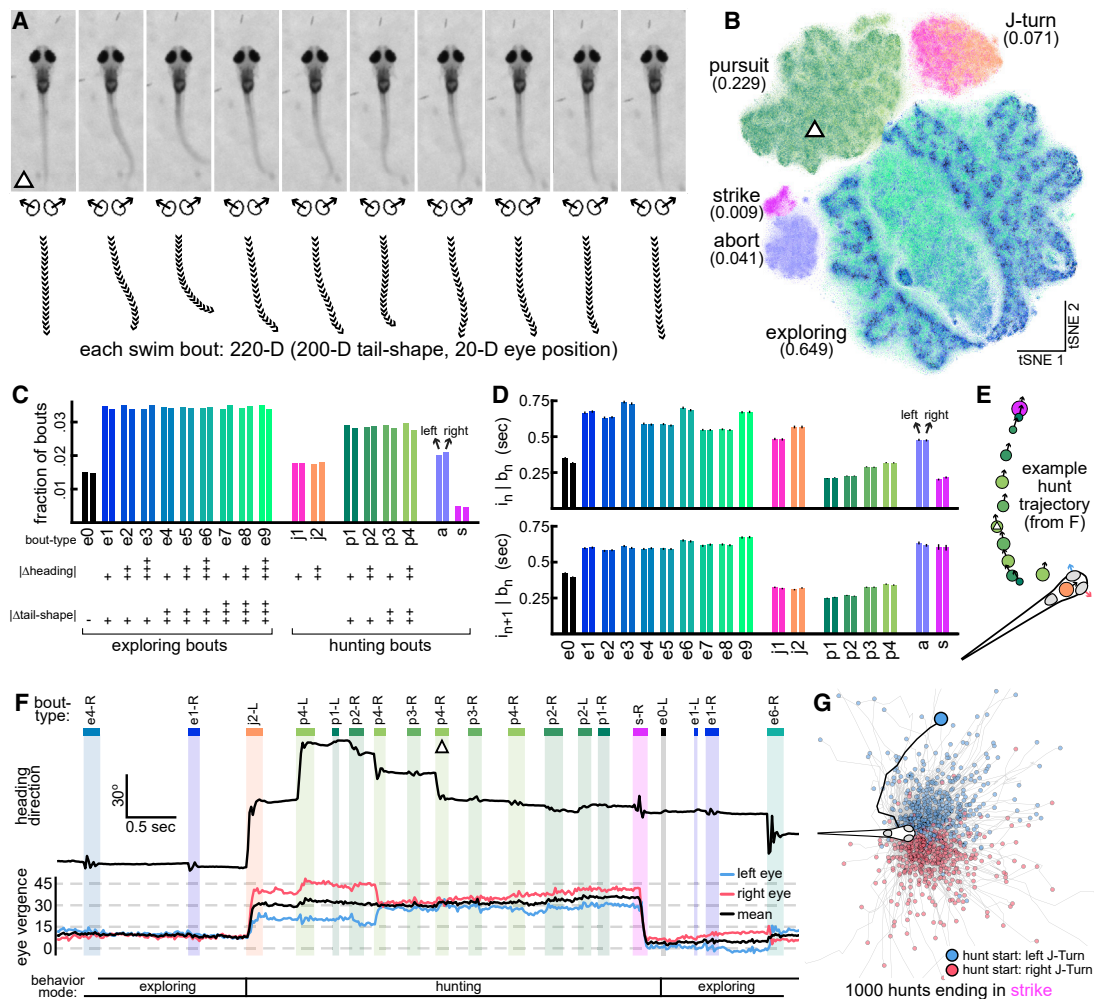


### Figure 2. Exploring and Hunting Bout-Type Categorization

(A) Bouts are represented as 10-frame postural sequences beginning at bout initiation. Bout shown immediately follows image from Figure 1J. (B) Bout dataset embedded in 2D space with tSNE. Five bout classes (abundances in parentheses) identified with density-based clustering (Figure S2). Location of bout from (A) indicated with triangle. Each bout is a point, colored by bout type (see C for colormap). (C) Large bout classes are subdivided to get bout types. Plus signs indicate kinematic parameter magnitude. (D) Duration (mean ± SE) of interbout intervals preceding (top) and following (bottom) left and right versions of each bout type. (E) Trajectory of 13-bout hunt ending in strike. Circle locations and arrows indicate head position and heading direction preceding bout initiation. Circle colors indicate bout type. Circle areas are proportional to  $|\Delta\text{tail shape}|$ . (F) Hunt from (E) contained in a longer bout sequence. Heading direction and eye vergence angles shown over time with bout and interbout epochs indicated. Bout from (A) indicated (triangle). See Video S2 for corresponding video data. (G) Trajectories from 1,000 complete hunts ending in strike (black line, hunt from E).

change per bout is narrowly and symmetrically distributed (Figure 1H). The arena contains abundant prey (mostly paramecia, some rotifers), and the fish tend to hunt prey near the water surface. Larvae converge their eyes during hunts to pursue prey with binocular vision. While not hunting, larvae keep their eyes more diverged, increasing visual coverage of the environment, which should improve threat detection. Larvae therefore experience a natural trade-off between seeking food and seeking safety. These opposing states are seen in the bimodal distribution of eye position measurements during interbout intervals (Figure 1I). We maintain a large circular field of view centered around the fish head (Figure 1J) with sufficient image sharpness to extract positions, sizes, shapes, and motion patterns of

objects near the water surface (Figure 1K). We later use this information to construct compressed representations of environmental state to predict the type of the next swim bout.

### Exploring and Hunting Bout-Type Categorization

To quantify behavioral sequence structure and compare across fed and starved groups, we first aim to categorize swim bouts into discrete types. We represent each swim bout as a 10-frame (167 ms) postural sequence beginning at bout initiation, giving a 220D egocentric representation of every bout (Figure 2A). We embed these observations in 2D space with tSNE [37, 38] (Figure 2B) and use density-based clustering [7, 39] to isolate five major classes of swim bouts (Figure S2). These classes consist

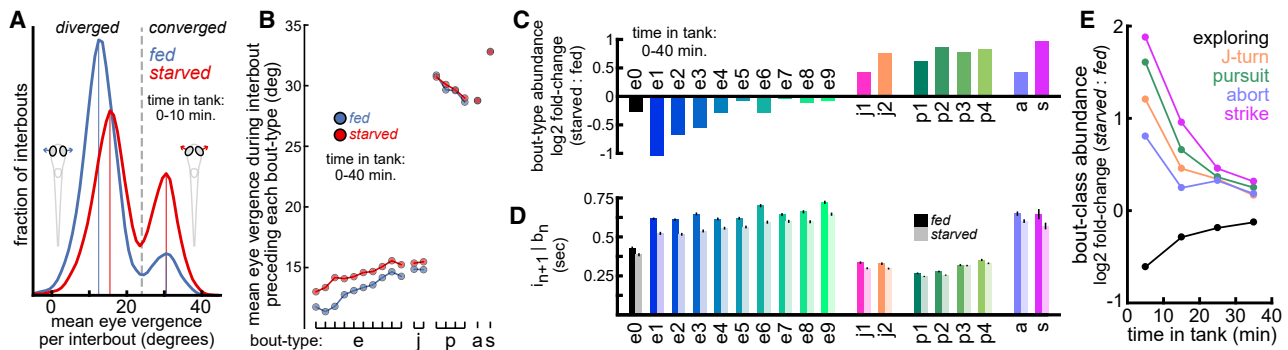


**Figure 3. Hunger Regulates Eye Position and Action Selection**

- (A) Mean eye vergence per interbout (like Figure 1) for observations in first 10 min of testing, shown separately for fed and starved groups. Solid vertical lines indicate local histogram peaks.
- (B) Fed fish display wider eye divergence preceding exploring bouts and J-turns, but not pursuits, aborts, and strikes (bout types ordered as in C). See Figure S3 for eye kinematics associated with each bout type.
- (C) Log<sub>2</sub> of relative bout-type abundances (starved/fed) during first 40 min of testing.
- (D) Interval durations (mean ± SE) following each bout type for fed and starved groups (first 40 min of testing).
- (E) Log<sub>2</sub> of relative bout-class abundances (starved/fed) in 10-min bins.

of hunting bouts (here called J-turn, pursuit, abort, and strike) and non-hunting bouts (here called exploring). Zebrafish larvae typically initiate hunts by converging their eyes and orienting toward prey with a J-turn [19], close distance to prey while maintaining eye convergence with pursuits [40] (also called approach [13] swims), and end hunts with eye divergence during a strike (also called capture [13] swim) or abort [41].

To improve analytical sensitivity, we further subdivide the three largest bout classes to yield ten exploring and eight hunting bout types (Figure 2C). Each bout type is symmetric with nearly equal numbers of leftward and rightward bouts. We use two scalar kinematic measurements to subdivide bout classes:  $|\Delta\text{heading}|$  and  $|\Delta\text{tail shape}|$ .  $|\Delta\text{heading}|$  is the magnitude of heading angle change per bout, and  $|\Delta\text{tail shape}|$  is the sum of the magnitudes of frame-to-frame changes in tail shape for each 10-frame bout representation (STAR Methods), a metric correlating with distance traveled per bout and presumably energy expenditure. See Figure S2 for detailed bout-type descriptions.

With labels assigned, the distributions of interbout intervals preceding and following each bout type are compared (Figures 2D). Larvae select longer intervals during exploration and shorter intervals during hunts. Distributions of intervals preceding (or following) left and right versions of each bout type are approximately equal, showing how left-right symmetry organizes population-level behavior. Larvae alternate between exploring and hunting modes, as seen in an example bout sequence containing a successful hunt (Figures 2E and 2F; Video S2). We define a complete hunt as a bout sequence beginning with J-turn, ending with abort or strike, and padded with only pursuits (for hunts longer than two bouts). The full dataset contains 7,230 complete hunts (19.6% end in strike). For comparison, the example hunt trajectory is shown with 999 other complete hunts ending in strike (Figure 2G).

### Hunger Regulates Eye Position and Action Selection

Feeding state strongly regulates larval zebrafish behavior, seen by comparing eye position histograms (as in Figure 1) across

fed and starved fish groups in the first 10 min of testing (Figure 3A). The fraction of intervals during which eyes are converged (threshold: mean vergence angle = 24°) is increased 183% from 0.124 in fed fish to 0.351 in starved fish in this time window. Fed fish also maintain wider eye divergence during exploration, but not while actively hunting (Figure 3B).

By comparing bout-type abundances and interbout intervals across fish groups in the first 40 min of testing, we find hunger affects larval zebrafish action selection in previously unreported ways. Fed fish upregulate use of low-energy exploring bouts (e1–3) relative to starved fish, with selection of the lowest displacement forward swim e1 increased 107% (Figure 3C). Starved fish are more likely to start hunts, especially through high-angle J-turns (j1 up 35%; j2 up 70%), and increase use of pursuits (up 71%), aborts (up 34%), and strikes (up 96%). Fed fish also produce longer intervals than starved fish, especially following low-energy exploring bouts (Figure 3D). Over ~40 min, behavioral patterns of fed and starved fish converge (Figure 3E) as their feeding states shift from opposing initial conditions (high hunger or high satiety) toward an intermediate state near nutrient equilibrium. To better quantify the behavioral sequences observed in this study, we next construct probabilistic models to predict the timing and type of swim bouts.

### Probabilistic Models to Predict Interbout Intervals

We model the data as a marked renewal process [31, 42], a stochastic process generating a sequence of discrete events in time, each characterized by an associated “mark” (Figure 4A). These statistical models specify the conditional distribution of the time and type of the next event in a sequence given the history of preceding events. First, we consider bout timing. Our key question for model construction is “what features of the event history carry predictive information about the timing of the next event?” We choose five interpretable features to represent behavioral history on multiple timescales (Figure 4B). On the shortest timescale, we model the interbout interval ( $i_n$ ) as a function of preceding bout type ( $b_{n-1}$ ) and preceding interbout

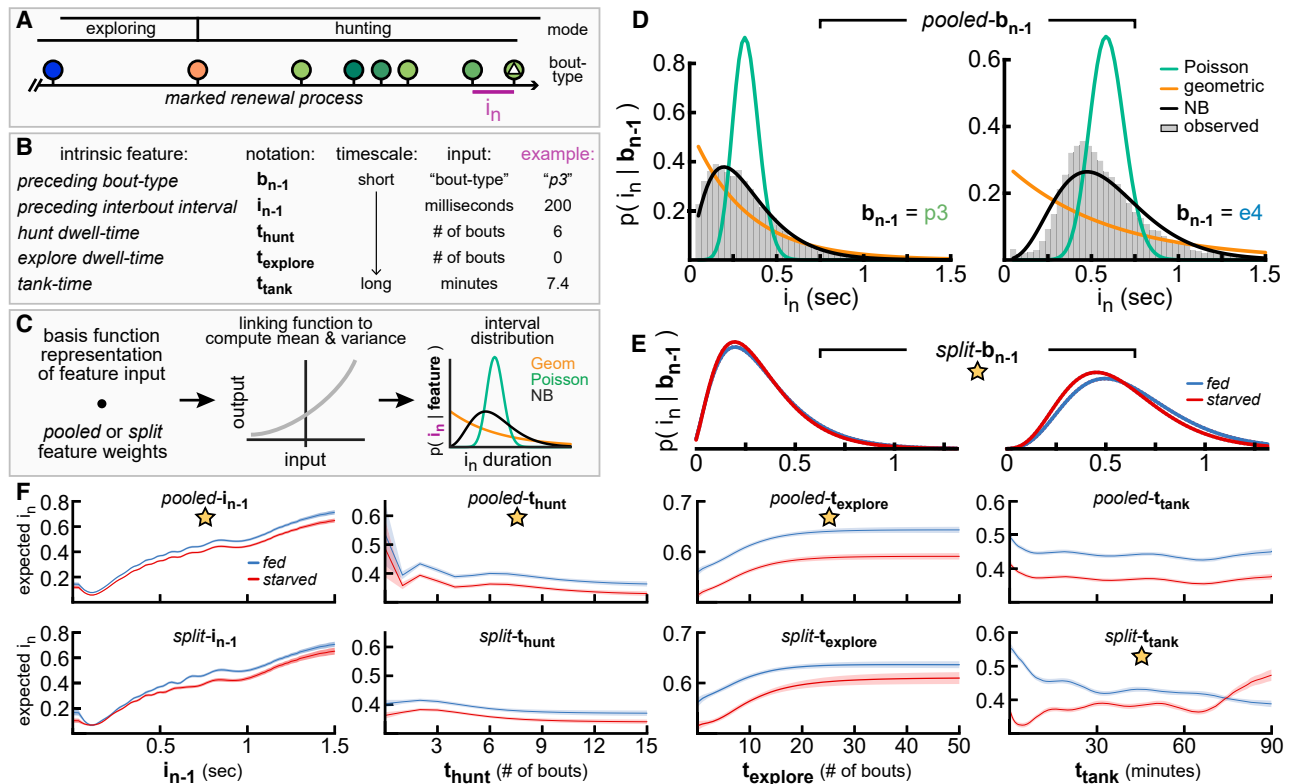


**Figure 4. Probabilistic Models to Predict Interbout Intervals**

(A) Behavioral data conceptualized as marked renewal process. Part of bout sequence from Figure 3F shown for example.

(B) Intrinsic features relate behavioral history and hunger to interval  $i_n$ . Example inputs to predict interval from (A) shown.

(C) Schematic of GLM to generate predictive probability distribution over  $i_n$ . Geometric and Poisson distributions are parameterized by just their mean, while the negative binomial distribution is also parameterized by variance.

(D)  $i_n$  probability distributions given two possible values for preceding bout type.

(E) Similar to (D), but for split- $b_{n-1}$  (NB distribution only).

(F) Predicted  $i_n$  (mean with 95% credible intervals) given from pooled and split forms of single-feature NB models.

interval ( $i_{n-1}$ ). On an intermediate timescale, we use hunt dwell time ( $t_{hunt}$ ) and explore dwell time ( $t_{explore}$ ) features to encode how long the fish has been hunting or exploring immediately prior to  $i_n$ . On the longest timescale, we encode how long the fish has been in the tank (tank time,  $t_{tank}$ ), relating how behavior changes with hunger. By comparing models composed from different features, we can learn how past actions predict future behavior.

Starved fish select shorter intervals than fed fish, but how else do patterns of bout timing differ? To interpret how feeding state influences relationships between behavioral history and interval selection, we consider two forms for each predictive feature: pooled and split. In pooled form, data from fed and starved fish are pooled to fit one set of weights relating that feature to  $i_n$ . In split form, separate weight sets are fit for each fish group. We use a generalized linear model [43] (GLM) with an exponential inverse link function to generate a probability distribution over  $i_n$  (Figure 4C). Briefly, the dot product of a basis function representation of the feature input with corresponding feature weights is computed and passed through an inverse link function to give the mean of a probability distribution over  $i_n$  (Methods S1). We considered three types of probability distributions over nonnegative counts: geometric, Poisson, and negative binomial (NB).

We find the NB distribution fits observed data best and consider this form throughout the paper.

For each model, we use an empirical Bayes [44] hyperparameter selection method (Methods S1) to choose an appropriate prior variance on weights, number of basis functions, and a preferred feature form (pooled or split, indicated with star). To model  $i_n$  given preceding bout type, separate NB distributions are fit for each possible value of  $b_{n-1}$  (two examples shown; Figure 4D). In split form, the  $b_{n-1}$  feature captures subtle differences in intervals produced by fed and starved fish (Figure 4E). For remaining features, we plot the predictive  $i_n$  mean for pooled and split models over a range of input values (Figure 4F). Each of these models includes additional split-bias weights to capture overall differences in interval mean and variance across groups (two extra free parameters per group: one for mean, one for variance). This design choice allows pooled feature models to capture basic group differences without using the more complex split features. On a short timescale, we find consecutive intervals are autocorrelated (column 1). On an intermediate timescale, intervals get shorter as hunt sequences get longer (column 2). By contrast, as exploring sequences get longer, intervals get longer (column 3). Aside from a shift in mean, the general relationship

between these features and  $i_n$  is similar across groups. By contrast, fed and starved fish display opposing interval selection patterns on the longest timescale (column 4). Starved fish initially hunt more, producing shorter intervals. Fed fish initially explore more, producing longer intervals. As their hunger states converge, intervals selected by fed and starved fish become more similar. These opposing patterns require the split- $t_{\text{tank}}$  feature to be modeled appropriately.

### Probabilistic Models to Predict Bout Types

The second component of the marked renewal process is a model of how the next bout type is selected depending on behavioral history, including the interval immediately preceding it. We add four extrinsic features to model how locations ( $v_{\text{loc}}$ ), sizes ( $v_{\text{size}}$ ), and relative velocities ( $v_x$ ,  $v_y$ ) of local environmental objects relate to bout-type selection (Figure 5A). We construct an 868D image ( $v_{\text{loc}}$ ) to encode putative prey object locations immediately preceding bout initiation. We modify  $v_{\text{loc}}$  to construct the other extrinsic features by scaling pixel intensities representing each object (Figure S4). We take the dot product of a basis function representation of a feature input with its corresponding weights to produce a vector of bout-type “activations,”  $\psi$  (Figure 5B). This vector is passed through a softmax function to generate a valid probability distribution,  $\pi$ , over all 36 possible bout types (Methods S1). As before, we select hyper-parameters and preferred feature forms, choosing pooled forms for all features except  $t_{\text{tank}}$ . As before, we include split-bias weights to account for differences in baseline bout-type abundances across fed and starved fish groups (36 extra free parameters per fish group).

Bout transition probabilities are captured by the preceding bout-type feature (Figures 5C and 5D). While exploring, larvae link consecutive bouts of similar energy (note increased transition probability along diagonal in Figure 5C). This may help larvae maintain speed [45] over many seconds, especially in combination with autocorrelated intervals. Larvae enter hunting mode with a transition to J-turn, after which they are likely to emit pursuits before an abort or strike. Since behavior is symmetric at the population level, we enforce feature symmetry to simplify and improve models. For example, the preceding bout-type feature encodes ipsilateral (Figure 5C) and contralateral (Figure 5D) bout transition probabilities. Larvae are known to link bouts in the same direction while exploring featureless environments [46], and we too see ipsilateral transitions are more probable. We find this pattern extends also to hunting, except for transitions into abort (Figure 5D, arrow), during which fish are likely to switch left-right state.

Prey object locations influence bout-type selection, especially during hunts, and pooled- $v_{\text{loc}}$  weights associated with each hunting bout type are shown (Figure 5E). Since  $v_{\text{loc}}$  inputs are high dimensional, we compress them by summing  $v_{\text{loc}}$  pixels within spatial bins as shown (Figure S4). Objects located in red bins increase the probability that the corresponding bout type will be selected next by the fish. Larvae typically select a J-turn to orient toward a laterally located object ( $\sim 15^\circ$ – $60^\circ$  relative to heading) and the magnitude of heading angle change depends on prey location [18] (compare j1 and j2). Energetic pursuits (p3–4) are more likely when prey are further away, while larger  $|\Delta\text{heading}|$  pursuits (p2, p4) are more likely when prey are

located more laterally. Prey locations affect how hunts end, with strike becoming most likely with an object located directly in front of the mouth. By contrast, aborts are weakly related to prey location and may be selected to terminate unsuccessful hunts. When prey are absent, exploring bouts become more probable since their associated  $v_{\text{loc}}$  weights are more spatially uniform with near-zero or negative values (data not shown).

The generative process underlying bout-type selection depends nonlinearly on preceding interbout interval. We capture this dependency with the pooled- $i_n$  model (Figure 5F). Activations ( $\psi$ ) of several bout types across the range of  $i_n$  input values are shown (left panel), with larger activations indicating higher bout-type probability. Full bout-type probability distributions evaluated at three specific  $i_n$  values are shown (panels i–iii), with probabilities across fed and starved fish averaged for display. At very short preceding interbout interval values ( $i_n < 0.25$  s), activations of p3, strike, and abort have different dynamics, indicating how timing is intricately involved in bout-type selection during hunts. As  $i_n$  extends from 0 to 0.25 s, strikes become less likely, aborts become more likely, and p3 probability peaks near 150 ms before decreasing again. As  $i_n$  reaches 0.5 s (panel ii), exploring bouts become more probable. As  $i_n$  reaches 1 s (panel iii), low-energy e1–3 and high- $|\Delta\text{heading}|$  e3, e6, and e9 bouts become most likely.

Longer timescale dependencies are captured with  $t_{\text{hunt}}$ ,  $t_{\text{explore}}$ , and  $t_{\text{tank}}$  features. As hunts extend, aborts become less likely and strikes become more likely (Figure 5G). Pursuits are always likely when larvae are in hunting mode (i.e.,  $t_{\text{hunt}}$  is non-zero), but the probability mass shifts toward the short straight p1 bout as hunts get longer and larvae approach a target. As explore dwell time increases, larvae become more likely to select low-energy exploring bouts and to remain in exploring mode (Figure 5H). J-turn emission probability decreases  $\sim 46\%$  as  $t_{\text{explore}}$  increases from 5 to 40 bouts. This may be partly explained by decreased food density as fish navigate toward the arena edge. On the longest timescale, the  $t_{\text{tank}}$  feature captures slow fluctuations in bout-type probabilities over the course of observation (Figure 5I). As with models of bout timing, the  $t_{\text{tank}}$  feature must be split to capture opposing behavioral trends of fed and starved fish on this timescale. Separate bout-type probability distributions for fed and starved fish are shown. These distributions become similar across groups as their hunger states converge at  $t_{\text{tank}} = 40$  min.

### Comparing and Combining Behavioral Models

Having constructed several single-feature models, we next compare their quality. We compute the marginal log likelihood (MLL) of each model and report improvement over the simplest baseline model (pooled bias). For interbout models, the baseline NB pooled-bias model has two parameters (one for mean, one for variance). For model comparison, we plot MLL for pooled and split forms of each model (Figure 6A). We include also  $b_{n-2}$  as well as  $i_{n-2}$ ,  $i_{n-3}$ ,  $i_{n-4}$ , and  $i_{n-5}$  to show how predictive information decays over time. We find preceding bout type is best able to predict  $i_n$ , but that preceding interbout interval is a close second, and that more distant behavioral history also provides useful information to model intervals. In general, MLL is similar across pooled and split forms, except for  $t_{\text{tank}}$ . We interpret this to suggest that any mild gains in predictive performance

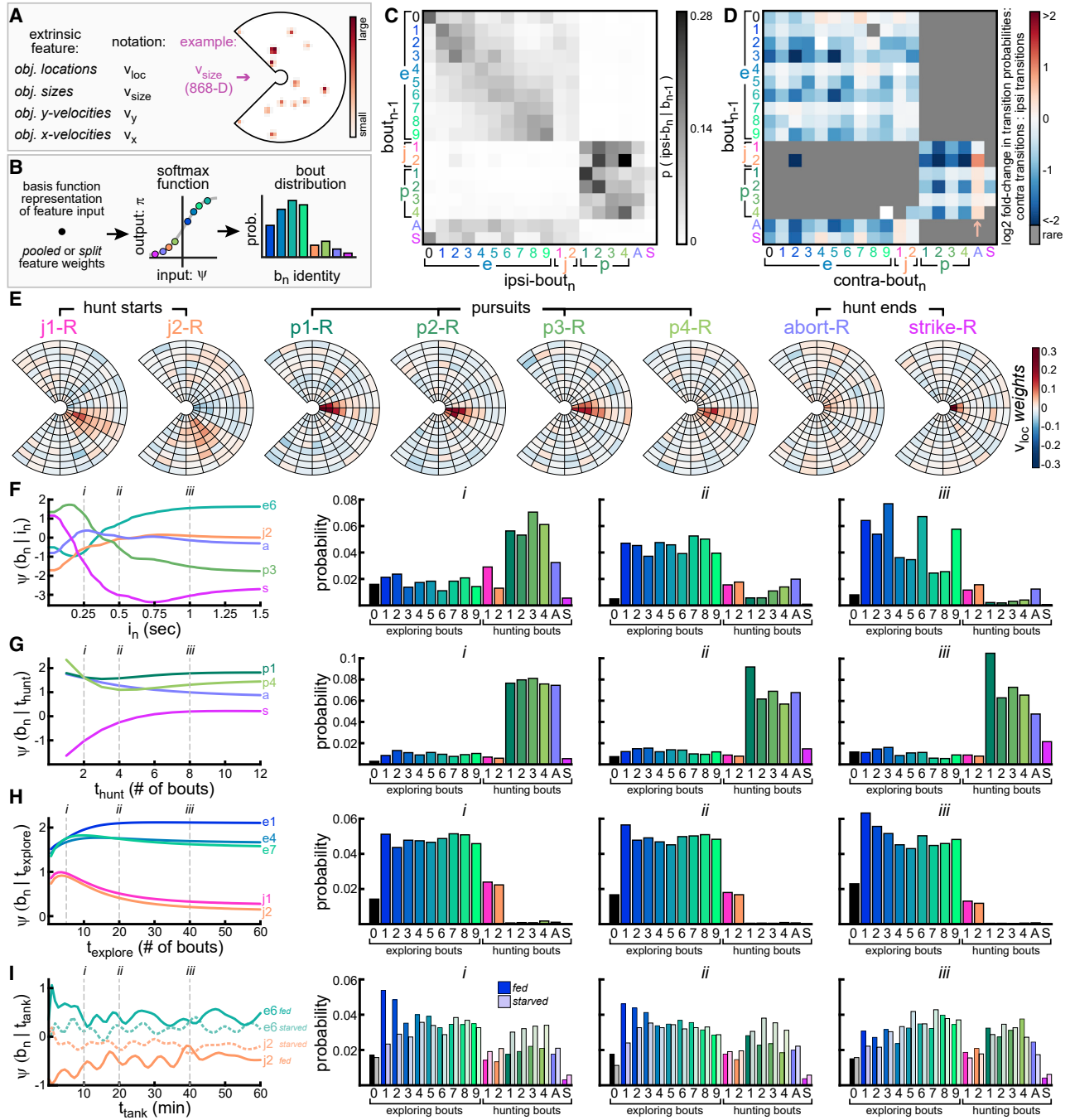


**Figure 5. Probabilistic Models to Predict Bout Types**

(A) Extrinsic features encode surface object locations and properties (see Figure S4). For example,  $v_{size}$  encodes object sizes (here, for objects from Figure 1K). (B) Schematic of GLM to generate predictive probability distribution over  $b_n$ . (C) Ipsilateral bout transition probabilities (i.e., left to left, or right to right) from pooled- $b_{n-1}$  model. Each row shows  $b_n$  probability given preceding bout type. (D) Contralateral bout transition probabilities (i.e., left to right, or right to left) from pooled- $b_{n-1}$  model, reported relative to ipsilateral transition probabilities. Rare transitions not shown. Blue squares indicate transitions that are more likely to occur ipsilaterally. Transitions into abort are more likely to occur contralaterally. (E) Weights from pooled- $v_{loc}$  model shown for each rightward hunting bout type. (F) Pooled- $i_n$  model summary. Activations of five bout types shown given preceding interbout interval. Full bout-type probability distribution evaluated at three specific  $i_n$  values (indicated with i, ii, iii). (G–I) Similar to (F), but for hunt dwell time (G), explore dwell time (H), and tank time (I). We choose the split architecture for tank time, with separate distributions for fed and starved fish shown.

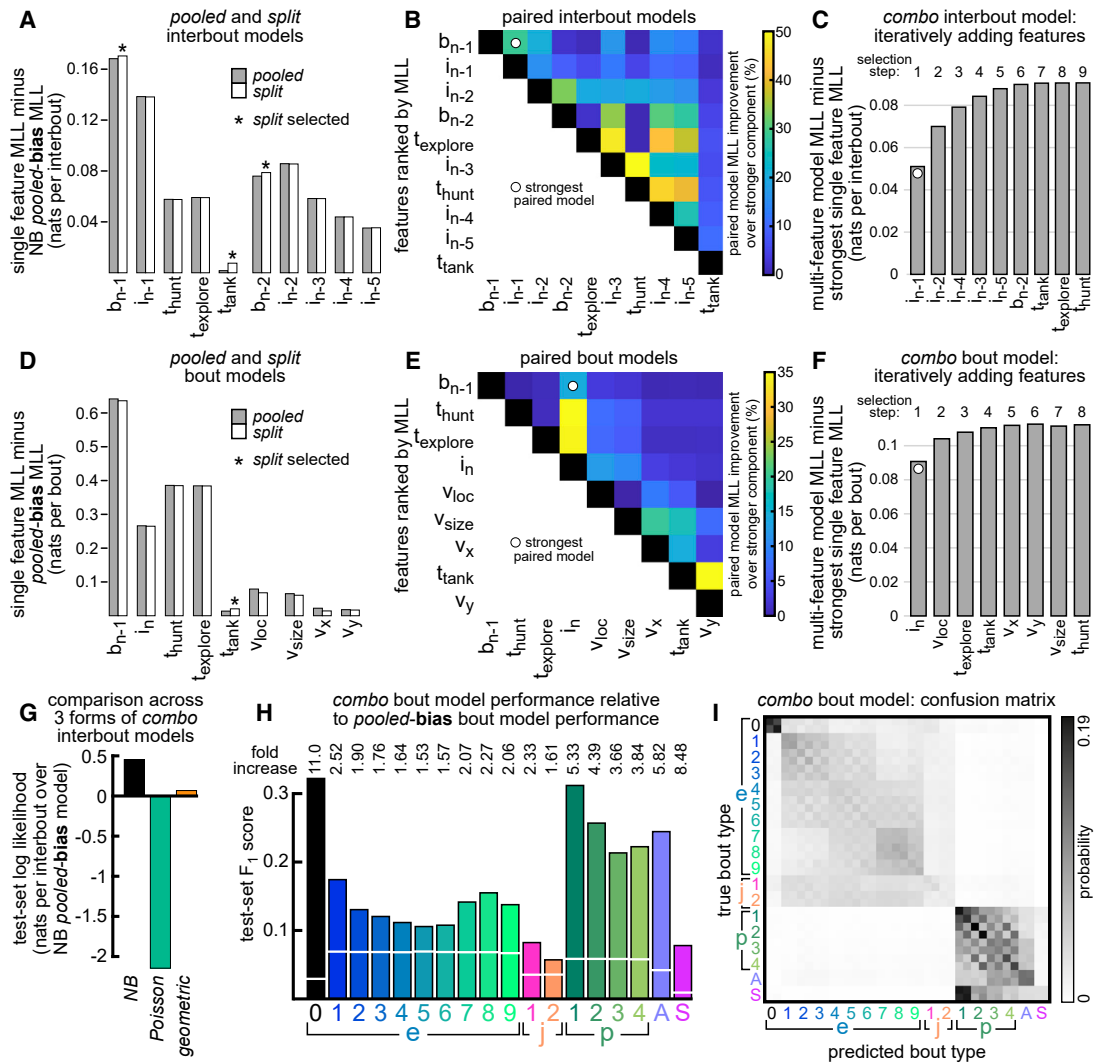


**Figure 6. Comparing and Combining Behavioral Models**

(A) Pooled and split single-feature NB interbout models compared by marginal log likelihood (MLL). MLL of simplest NB interbout model (pooled bias) subtracted from each model's MLL as baseline. For comparison, we include features similar to preceding bout type and preceding interbout interval, but from further into behavioral history. Pooled forms selected unless indicated.

(B) All pairwise combinations of features (in selected form) are used to make 45 paired interbout models. Paired model MLL calculated as in (A) (i.e., baseline-subtracted) and divided by baseline-subtracted MLL of stronger feature component.

(C) All features combined to make combo GLM for intervals. Starting with strongest paired model, we add the feature at each selection step that increases MLL most, until all features are added.

(D–F) Same as (A)–(C), but for bout-type models. See Figure S5 for information on extrinsic feature neural network models.

(G) NB combo interbout model compared to similarly constructed combo geometric or Poisson models to predict  $i_n$ . NB distribution fits the data best.

(H) Performance of combo bout model compared to baseline (pooled-bias model captures only overall bout-type abundances).  $F_1$ -statistic computed for each bout type on test-set data (combo model, bars; baseline, white lines). Fold increase shown for each bout type. See Figure S6 for similar analyses of single-feature bout models.

(I) Combo bout model confusion matrix (separate rows for left and right versions of each bout type). Each row sums to one, showing average model output for all bouts of that type in test set.

through use of split features may be offset by increased complexity and decreased training examples per split weight.

While preceding bout type is the best predictor of  $i_n$ , can we build stronger models by combining features? We approach this question by combining all pairs of features (in their selected forms) to produce 45 paired interbout GLMs (Figure 6B). For each paired model, we compute MLL and report improvement

over the stronger component. Paired models showing large improvement should combine features that provide some unique information about interbout  $i_n$ . We find preceding bout type and preceding interbout interval combine to produce the strongest paired interbout model. This paired  $[b_{n-1}, i_{n-1}]$  model improves over  $b_{n-1}$  alone by 0.05 nats per interbout, or 29% relative to baseline. By contrast, the  $[b_{n-1}, t_{explore}]$  model improves over

$\mathbf{b}_{n-1}$  by just 0.002 nats per interbout, or 1.4%. Since models can improve by combining features, we combine all features to construct a combo interbout model (Figure 6C). Features are added sequentially via greedy stepwise selection, adding the feature that increases MLL most at each step. Model quality improves and saturates during construction.

We repeat this procedure for bout-type models. We find preceding bout type is by far the best predictor of bout type  $\mathbf{b}_n$ , followed by hunt dwell time and explore dwell time, and then preceding interbout interval (Figure 6D). As constructed, our extrinsic feature GLMs fail to fully capture the complex relationship between environmental state and bout-type selection. This problem is challenging for several reasons. Identified objects include both prey and non-prey (e.g., dust, algae), which differentially influence behavior. Second, environmental objects are highly abundant in these experiments (mean number of identified objects per bout = 12), complicating the visual scenes experienced by the fish and also our environmental representations. Third, the locations, sizes, shapes, and motion patterns of objects are likely to interact in complex ways to influence larval zebrafish action selection. To improve our understanding of how sensory input relates to bout-type selection, we construct feedforward neural networks that take extrinsic feature inputs (Figure S5) and combine them nonlinearly to form a prediction. We find this neural network model improves substantially over the  $\mathbf{v}_{loc}$  GLM, with predictions of all bout types improving on held-out data, especially hunting bouts. However, bout type  $\mathbf{b}_n$  is still far better predicted by preceding bout type, indicating more sophisticated modeling approaches will be needed to better predict future behavior from complex environmental data, but also that bout-type selection depends strongly on the animal's short-term behavioral history [1].

The strongest paired bout model again combines preceding bout type with preceding interbout interval, even though preceding interbout interval is just the 4<sup>th</sup> strongest individual feature (Figure 6E). This paired  $[\mathbf{b}_{n-1}, i_n]$  model improves over  $\mathbf{b}_{n-1}$  alone by 0.09 nats per bout, or 14%. By contrast, the paired  $[\mathbf{b}_{n-1}, \mathbf{t}_{explore}]$  model improves over  $\mathbf{b}_{n-1}$  by just 0.005 nats per bout, or 0.8%. This result again indicates that distinct features of the fish's short-term behavioral history (i.e., preceding bout type and preceding interbout interval) encode non-redundant information about future action selection. As before, we construct a combo bout model through greedy stepwise selection (Figure 6F). The strongest three-component bout model ( $[\mathbf{b}_{n-1}, i_n, \mathbf{v}_{loc}]$ ) adds information about prey locations to the strongest paired bout model, combining internal and external information over a timescale of a second or less.

We next examine combo model quality. To confirm the NB distribution is warranted, we compare our NB combo interbout model to similar combo models constructed instead with Poisson or geometric distributions (Figure 6G). While requiring more free parameters, the NB model clearly outperforms the others on held-out data. For the combo bout model, we show its ability to predict each individual bout type, as measured by the  $F_1$  score [47] of each one-versus-rest classifier, and compare this performance to baseline (Figure 6H). This shows us which bout types are easiest to predict (e.g., pursuits, aborts, strikes, e0), and which are most challenging (e.g., e4–6, j2). We reproduce this analysis for several single-feature bout models as

well as the strongest paired and three-component bout models (Figure S6). The combo bout model distributes probability mass over similar bout types (Figure 6I), which should be expected if the generative processes involved in producing similar bout types are also similar.

### Simulating Trajectories of Fed and Starved Fish

A strong test of a behavioral model is to evaluate its ability to generate realistic behavior in novel contexts. To that end, we alternate sampling from our combo bout and interbout models (here called a combo renewal process) to move a virtual fish through an artificial environment with abundant prey (Figure 7A; Videos S3 and S4). We simulated trajectories of fed and starved fish to capture multiple timescales of structure in larval zebrafish behavior. Prey object locations influence hunting bout selection in expected ways (Figure 7B) and fed fish select longer intervals (Figure 7C), as expected. The strong effects of hunger are seen by comparing bout transition probabilities of simulated fed and starved fish (Figure 7D). Fed fish are more likely to transition to low-energy exploring bouts, while starved fish are more likely to transition to high-energy exploring bouts. Starved fish also adjust their behavior in several ways to increase food intake. They are more likely to transition to J-turns (especially j2) and to extend hunt sequences by linking pursuits [41]. Starved fish are also less likely to transition to abort and more likely to transition to strike.

These simulations also capture longer timescale behavioral dependencies observed in our experiments. With real fish, we find hunts ending in strike are much longer than those ending in abort (Figure 7E). This trend is absent in simulations generated from a first-order Markov renewal process in which intervals and bout types depend on just preceding bout type ( $\mathbf{b}_{n-1}$ ). By contrast, combo renewal process simulations do better to recover this higher-order hunting structure. Our simulations also capture non-Markovian dynamics during exploration (e.g., decreased J-turn probability as exploring sequences lengthen; data not shown). Finally, our model reproduces slowly changing bout-type selection probabilities across fed and starved fish as their hunger states converge over 40 min (Figure 7F).

## DISCUSSION

Behavior is the principal output of the nervous system and is complex and high dimensional [48, 49]. To make studying the brain more manageable, behavior is often constrained in neuro-behavioral experiments. This reductionist approach has many benefits: it simplifies behavioral description, reduces experimental variability, and improves interpretability of neural data. However, an important frontier in neuroscience is to better understand how brains function in natural conditions [50]. The NIH BRAIN Initiative [51] has identified study of the “Brain In Action” [52] as a priority research area, stating that “a critical step ahead is to study more complex behavioral tasks and to use more sophisticated methods of quantifying behavioral, environmental, and internal state influences on individuals” [53]. Importantly, these methods should capture dynamics of minimal behavioral elements, scale to big datasets, and be compatible with modern techniques to record neural population activity. Here we describe such an approach to predict and simulate natural larval zebrafish behavior. Further, by constructing a model of

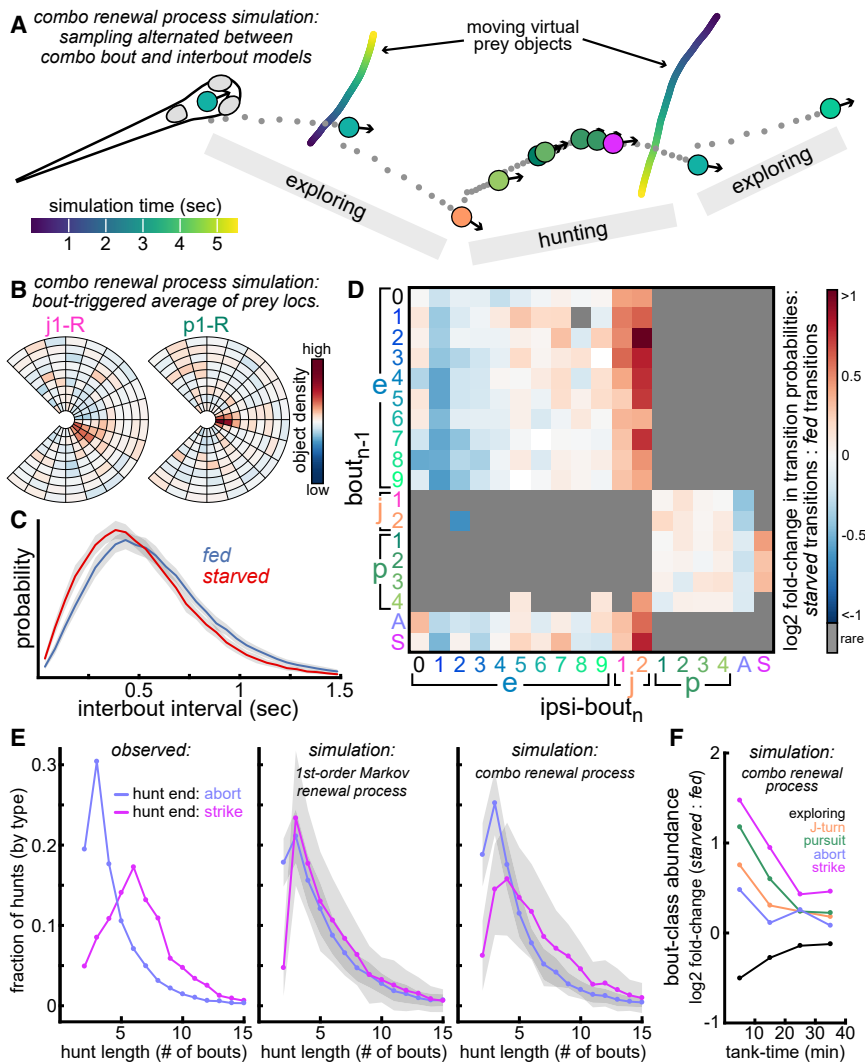


**Figure 7. Simulating Trajectories of Fed and Starved Fish**

(A) We simulate behavioral trajectories of 50 fed and 50 starved fish (40 min per fish) by alternating sampling from combo interbout and bout models (here called a combo renewal process). Approximately 5 s of simulated behavior shown in which fish hunts and strikes at a virtual prey. See [Video S3](#) for animation of this simulated sequence and [Video S4](#) for visualization of how these bout types and intervals were selected from conditional probability distributions evolving over time. Fish move through the environment using bout-type trajectories shown in [Figure S7](#). Virtual prey move through environment as biased random-walking particles with fixed sizes and speeds.

(B) Bout-type triggered averages of fish FOV preceding initiation of two bout types.

(C) Histograms of simulated interval durations (mean  $\pm$  SE).

(D) Ipsilateral bout transition probabilities of simulated fed and starved fish are compared. Red squares indicate increased transition probability for starved fish relative to fed fish.

(E) Hunt length distributions for complete hunts ending in strike or abort. Left panel: all complete hunts observed from real fish. Middle panel: all complete hunts (mean  $\pm$  SE across fish) from simulations in which bout types and intervals depend on only preceding bout type (called a first-order Markov renewal process). Right panel: all complete hunts (mean  $\pm$  SE across fish) from combo renewal process simulations.

(F) Relative bout-class abundances produced in combo renewal process simulations (similar to [Figure 3E](#)).

(e.g., optic tectum, AF7) [56, 57]. If so, retinal output may be processed asymmetrically to promote ipsilateral transitions from exploring to hunting.

how state influences action, we can make predictions about what types of signals must be present in the neural system driving this behavior.

Our study generates testable hypotheses about how neural mechanisms might give rise to observed behavioral patterns on multiple timescales. On a short timescale, we see larvae are likely to link consecutive exploring bouts through ipsilateral transitions, but also tend to begin hunts ipsilaterally. It has been shown that reciprocally connected circuits in the anterior hindbrain (anterior rhombencephalic turning region; ARTR) alternate between “leftward” and “rightward” states to mediate temporal correlations in turn direction during exploration [46], but how ARTR or related circuits may bias reactions to prey stimuli is unknown. We predict ARTR projections may asymmetrically modulate premotor systems (e.g., reticulospinal neurons [54], hunting command neurons [55], or premotor tectal assemblies [56]) such that, with the ARTR in a leftward state, leftward J-turns are generated preferentially to rightward J-turns. Alternatively, ARTR-state-dependent modulation could occur further upstream in the sensorimotor hierarchy through asymmetric modulation of retinorecipient areas processing prey stimuli

Following hunt initiation, several behavioral patterns interact to influence hunt outcome. As hunts extend, larvae select shorter intervals, pursuits become finer, and abort probability decreases while strike probability increases. By contrast, as intervals extend, abort probability increases, pursuit probability rises and falls, and strike probability decreases. These time-sensitive patterns likely depend on reciprocal connectivity between the nucleus isthmi (NI) and (pre)tectum. It has been shown that NI neurons become active following hunt initiation and that NI ablation leads to specific deficits in hunt sequence maintenance [41]. Henriques et al. [41] propose NI-mediated feedback facilitation of (pre)tectal prey responses increases hunt sequence extension probability. This mechanism may explain why abort probability decreases and strike probability increases as hunts elongate in our study. However, how hunting bout-type selection depends so precisely on bout timing is not well understood. We posit tectal prey representations may attenuate as intervals extend past a few hundred milliseconds, potentially through phasic bout-locked NI feedback that decreases as intervals elongate. Alternatively, premotor populations [34, 55, 56] involved in pursuit and strike generation may become increasingly inhibited

as interbouts get longer, increasing hunt termination probability. Also, since larvae tend to abort hunts through contralateral transitions, we suspect abort generation may frequently coincide with a change in ARTR state. Such a mechanism could facilitate switches in spatial attention from one hemifield to the other, thereby inhibiting return [58] to a previously pursued object.

Hunger state affects larval zebrafish behavior in many ways. We see starved fish are more likely to initiate and extend hunts. They also upregulate transitions to strike and downregulate transitions to abort relative to fed fish. It has been shown that food deprivation modulates larval zebrafish tectal processing of prey-like and predator-like visual stimuli such that food-deprived larvae are more likely to approach small moving dots [35]. Specifically, hunger induces recruitment of additional prey-responsive tectal neurons and neuroendocrine and serotonergic signaling mediates this effect [35]. We posit this mechanism may increase tectal input to NI, thereby increasing NI-mediated feedback to facilitate hunt sequence extension and increased strike probability in starved fish. While not yet tested, direct hunger-state modulation of tectal-projecting NI neurons is also plausible. Other studies show that lateral hypothalamic neuron activity correlates positively with feeding rate [59] and that lateral hypothalamic neurons respond to both sensory and consummatory food cues [60]. This brain region is likely critically involved in sustaining increased hunting over tens of minutes through modulating visual responses to prey and/or facilitating hunting (pre)motor circuits.

While the above mechanisms can explain why fed fish initiate fewer hunts, we posit satiety signals affect additional circuits to further improve safety against predation during exploration. Fed fish select longer interbout intervals, lower-energy exploring bouts, and maintain wider eye divergence during exploration. These strategies could improve safety by decreasing their visibility to predators (by moving less) and increasing their ability to detect threats (by widening surveillance). To coordinate these behavioral patterns, satiety cues may separately modulate midbrain nuclei involved in regulating bout timing [61], nMLF neurons involved in regulating swim bout duration and tail-beat frequency [45], and oculomotor centers involved in controlling eye position [62–64]. It is clear that feeding state coordinates a complex array of behavioral modifications, likely through modulation of many circuits distributed across the larval zebrafish brain.

There are many avenues to extend this work. In future studies, moving camera systems should use faster camera frame rates, shorter exposure durations, and better tracking algorithms to improve raw behavioral data. These adjustments will allow for higher resolution pose estimation (e.g., by including pectoral fin dynamics, pitch and roll estimates, and tail half-beat analysis [13]), facilitate more comprehensive bout-type classification, and yield significantly longer continuous behavioral sequences. Richer datasets will enable future models to extract nuanced environmental dependencies, like prolonged attention to single prey among many distractors [65]. Future models may simultaneously infer discrete behavioral states and their dynamics [7, 14, 66, 67], though the non-Markovian dependencies on past behavior present new challenges [68]. Likewise, there are many other internal state variables governing action selection, and future models could seek to infer these latent states [68]

rather than using proxy covariates like tank time. Behavioral states and dynamics differ slightly from one individual larva to the next, and long-term behavioral recordings combined with hierarchical models [69, 70] will allow us to study how these behavioral differences emerge and change throughout early development. The contribution of particular neural populations in generating naturalistic behavioral patterns may also be probed by combining our behavioral models with experiments to activate, inhibit, or ablate specific neural cell types in observed fish. Finally, our approach may be combined with new technologies to record large neural populations in freely swimming fish [71–75]. This will present opportunities to construct joint models of neural activity and natural behavior that are likely to improve the predictability of behavioral sequences while providing important new tools to study the brain in action [76, 77].

## STAR★METHODS

Detailed methods are provided in the online version of this paper and include the following:

- KEY RESOURCES TABLE
- LEAD CONTACT AND MATERIALS AVAILABILITY
- EXPERIMENTAL MODEL AND SUBJECT DETAILS
- METHOD DETAILS
  - BEAST Design
  - Data Acquisition
  - Statistical Models
- QUANTIFICATION AND STATISTICAL ANALYSIS
  - Image Registration and Fish Pose Estimation
  - Temporal Segmentation of Bout and Interbout Epochs
  - Bout Summary Statistics
  - tSNE Input
  - Identifying and Encoding Environmental Information
  - Intrinsic Features to Predict Interbout Intervals and Bout-types
  - Extrinsic Features to Predict Bout-types
  - Simulations
- DATA AND CODE AVAILABILITY

## SUPPLEMENTAL INFORMATION

Supplemental Information can be found online at <https://doi.org/10.1016/j.cub.2019.11.026>.

## ACKNOWLEDGMENTS

Research was funded by NIH grants U19NS104653, R43 OD024879, R24 NS086601, and 2R44OD024879 and Simons Foundation grants SCGB-325207 and SCGB-542973. S.L. was supported by a Simons Collaboration on the Global Brain postdoctoral fellowship (SCGB-418011) and the Siebel Scholarship. We thank Ed Soucy, Joel Greenwood, and Adam Bercu of the Harvard Center for Brain Science Neuroengineering Core for technical support. We thank Andrew Bolton for helpful discussions on pose estimation and prey quantification, George Dimitriadis and Adam Kampff for assistance with GPU implementation of tSNE, and Matthew Johnson for helpful modeling discussions.

## AUTHOR CONTRIBUTIONS

R.E.J. and F.E. conceived the project. T.P. and R.E.J. designed and constructed BEAST. R.E.J. and C.L.W. conceived the basic experimental design.

R.E.J. wrote the data acquisition code. R.E.J., C.L.W., and E.S. collected the data. R.E.J. processed and prepared all data for use in modeling studies. S.L. conceived and implemented all models with input from R.E.J. A.M. advised on neural network models. K.J.H. made the animations in Videos S1 and S3. R.E.J. wrote the paper with input from all authors. S.L., C.L.W., K.J.H., and F.E. edited the paper. S.L. wrote the Technical Appendix (Methods S1).

## DECLARATION OF INTERESTS

The authors declare no competing interests.

Received: July 22, 2019

Revised: September 11, 2019

Accepted: November 7, 2019

Published: December 19, 2019

## REFERENCES

- Brown, A.E., and De Bivort, B. (2018). Ethology as a physical science. *Nat. Phys.* *14*, 653–657.
- Stephens, G.J., Johnson-Kerner, B., Bialek, W., and Ryu, W.S. (2008). Dimensionality and dynamics in the behavior of *C. elegans*. *PLoS Comput. Biol.* *4*, e1000028.
- Swierczek, N.A., Giles, A.C., Rankin, C.H., and Kerr, R.A. (2011). High-throughput behavioral analysis in *C. elegans*. *Nat. Methods* *8*, 592–598.
- Yemini, E., Jucikas, T., Grundy, L.J., Brown, A.E., and Schafer, W.R. (2013). A database of *Caenorhabditis elegans* behavioral phenotypes. *Nat. Methods* *10*, 877–879.
- Gyenes, B., and Brown, A.E. (2016). Deriving shape-based features for *C. elegans* locomotion using dimensionality reduction methods. *Front. Behav. Neurosci.* *10*, 159.
- Vogelstein, J.T., Park, Y., Ohyama, T., Kerr, R.A., Truman, J.W., Priebe, C.E., and Zlatic, M. (2014). Discovery of brainwide neural-behavioral maps via multiscale unsupervised structure learning. *Science* *344*, 386–392.
- Berman, G.J., Choi, D.M., Bialek, W., and Shaevitz, J.W. (2014). Mapping the stereotyped behaviour of freely moving fruit flies. *J. R. Soc. Interface* *11*, 20140672.
- Klibaite, U., Berman, G.J., Cande, J., Stern, D.L., and Shaevitz, J.W. (2017). An unsupervised method for quantifying the behavior of paired animals. *Phys. Biol.* *14*, 015006.
- Girdhar, K., Gruebele, M., and Chemla, Y.R. (2015). The behavioral space of zebrafish locomotion and its neural network analog. *PLoS ONE* *10*, e0128668.
- Burgess, H.A., and Granato, M. (2007). Modulation of locomotor activity in larval zebrafish during light adaptation. *J. Exp. Biol.* *210*, 2526–2539.
- Mirat, O., Sternberg, J.R., Severi, K.E., and Wyart, C. (2013). ZebraZoom: an automated program for high-throughput behavioral analysis and categorization. *Front. Neural Circuits* *7*, 107.
- Jouary, A., and Sumbre, G. (2016). Automatic classification of behavior in zebrafish larvae. *bioRxiv*. <https://doi.org/10.1101/052324>.
- Marques, J.C., Lackner, S., Félix, R., and Orger, M.B. (2018). Structure of the zebrafish locomotor repertoire revealed with unsupervised behavioral clustering. *Curr. Biol.* *28*, 181–195.e5.
- Wiltshchko, A.B., Johnson, M.J., Iurilli, G., Peterson, R.E., Katon, J.M., Pashkovski, S.L., Abaira, V.E., Adams, R.P., and Datta, S.R. (2015). Mapping sub-second structure in mouse behavior. *Neuron* *88*, 1121–1135.
- Mathis, A., Mamidanna, P., Cury, K.M., Abe, T., Murthy, V.N., Mathis, M.W., and Bethge, M. (2018). DeepLabCut: markerless pose estimation of user-defined body parts with deep learning. *Nat. Neurosci.* *21*, 1281–1289.
- Pereira, T.D., Aldarondo, D.E., Willmore, L., Kislin, M., Wang, S.S.H., Murthy, M., and Shaevitz, J.W. (2019). Fast animal pose estimation using deep neural networks. *Nat. Methods* *16*, 117–125.
- Graving, J.M., Chae, D., Naik, H., Li, L., Koger, B., Costelloe, B.R., and Couzin, I.D. (2019). DeepPoseKit, a software toolkit for fast and robust animal pose estimation using deep learning. *eLife* *8*, e47994.
- Patterson, B.W., Abraham, A.O., MacIver, M.A., and McLean, D.L. (2013). Visually guided gradation of prey capture movements in larval zebrafish. *J. Exp. Biol.* *216*, 3071–3083.
- Bianco, I.H., Kampff, A.R., and Engert, F. (2011). Prey capture behavior evoked by simple visual stimuli in larval zebrafish. *Front. Syst. Neurosci.* *5*, 101.
- Portugues, R., and Engert, F. (2011). Adaptive locomotor behavior in larval zebrafish. *Front. Syst. Neurosci.* *5*, 72.
- Oteiza, P., Odstrcil, I., Lauder, G., Portugues, R., and Engert, F. (2017). A novel mechanism for mechanosensory-based rheotaxis in larval zebrafish. *Nature* *547*, 445–448.
- Haesemeyer, M., Robson, D.N., Li, J.M., Schier, A.F., and Engert, F. (2015). The structure and timescales of heat perception in larval zebrafish. *Cell Syst.* *1*, 338–348.
- Naumann, E.A., Fitzgerald, J.E., Dunn, T.W., Rihel, J., Sompolinsky, H., and Engert, F. (2016). From whole-brain data to functional circuit models: the zebrafish optomotor response. *Cell* *167*, 947–960.e20.
- Colwill, R.M., and Creton, R. (2011). Imaging escape and avoidance behavior in zebrafish larvae. *Rev. Neurosci.* *22*, 63–73.
- Lacoste, A.M., Schoppik, D., Robson, D.N., Haesemeyer, M., Portugues, R., Li, J.M., Randlett, O., Wee, C.L., Engert, F., and Schier, A.F. (2015). A convergent and essential interneuron pathway for Mauthner-cell-mediated escapes. *Curr. Biol.* *25*, 1526–1534.
- Dunn, T.W., Gebhardt, C., Naumann, E.A., Riegler, C., Ahrens, M.B., Engert, F., and Del Bene, F. (2016). Neural circuits underlying visually evoked escapes in larval zebrafish. *Neuron* *89*, 613–628.
- Dreosti, E., Lopes, G., Kampff, A.R., and Wilson, S.W. (2015). Development of social behavior in young zebrafish. *Front. Neural Circuits* *9*, 39.
- Truccolo, W., Eden, U.T., Fellows, M.R., Donoghue, J.P., and Brown, E.N. (2005). A point process framework for relating neural spiking activity to spiking history, neural ensemble, and extrinsic covariate effects. *J. Neurophysiol.* *93*, 1074–1089.
- Cunningham, J.P., Yu, B.M., Sahani, M., and Shenoy, K.V. (2007). Inferring neural firing rates from spike trains using Gaussian processes. *Adv. Neural Inf. Process. Syst.* *20*, 329–336.
- Pillow, J.W., Shlens, J., Paninski, L., Sher, A., Litke, A.M., Chichilnisky, E.J., and Simoncelli, E.P. (2008). Spatio-temporal correlations and visual signalling in a complete neuronal population. *Nature* *454*, 995–999.
- Kass, R.E., Eden, U.T., and Brown, E.N. (2014). *Analysis of Neural Data* Volume 491 (Springer).
- Jordi, J., Guggiana-Nilo, D., Soucy, E., Song, E.Y., Lei Wee, C., and Engert, F. (2015). A high-throughput assay for quantifying appetite and digestive dynamics. *Am. J. Physiol. Regul. Integr. Comp. Physiol.* *309*, R345–R357.
- Jordi, J., Guggiana-Nilo, D., Bolton, A.D., Prabha, S., Ballotti, K., Herrera, K., Rennekamp, A.J., Peterson, R.T., Lutz, T.A., and Engert, F. (2018). High-throughput screening for selective appetite modulators: A multibehavioral and translational drug discovery strategy. *Sci. Adv.* *4*, v1966.
- Barker, A.J., and Baier, H. (2015). Sensorimotor decision making in the zebrafish tectum. *Curr. Biol.* *25*, 2804–2814.
- Filosa, A., Barker, A.J., Dal Maschio, M., and Baier, H. (2016). Feeding state modulates behavioral choice and processing of prey stimuli in the zebrafish tectum. *Neuron* *90*, 596–608.
- Huang, K.H., Ahrens, M.B., Dunn, T.W., and Engert, F. (2013). Spinal projection neurons control turning behaviors in zebrafish. *Curr. Biol.* *23*, 1566–1573.
- Maaten, L.d., and Hinton, G. (2008). Visualizing data using t-SNE. *J. Mach. Learn. Res.* *9*, 2579–2605.
- Dimitriadis, G., Neto, J.P., and Kampff, A.R. (2018). T-SNE visualization of large-scale neural recordings. *Neural Comput.* *30*, 1750–1774.

39. Todd, J.G., Kain, J.S., and de Bivort, B.L. (2017). Systematic exploration of unsupervised methods for mapping behavior. *Phys. Biol.* *14*, 015002.
40. Gahtan, E., Tanger, P., and Baier, H. (2005). Visual prey capture in larval zebrafish is controlled by identified reticulospinal neurons downstream of the tectum. *J. Neurosci.* *25*, 9294–9303.
41. Henriques, P.M., Rahman, N., Jackson, S.E., and Bianco, I.H. (2019). Nucleus isthmi is required to sustain target pursuit during visually guided prey-catching. *Curr. Biol.* *29*, 1771–1786.e5.
42. Daley, D.J., and Vere-Jones, D. (2003). *An Introduction to the Theory of Point Processes: Volume I: Elementary Theory and Methods* (Springer-Verlag).
43. McCullagh, P., and Nelder, J. (1989). *Generalized Linear Models*, Second Edition (Chapman & Hall).
44. Carlin, B.P., and Louis, T.A. (2010). *Bayes and Empirical Bayes Methods for Data Analysis* (Chapman & Hall).
45. Severi, K.E., Portugues, R., Marques, J.C., O'Malley, D.M., Orger, M.B., and Engert, F. (2014). Neural control and modulation of swimming speed in the larval zebrafish. *Neuron* *83*, 692–707.
46. Dunn, T.W., Mu, Y., Narayan, S., Randlett, O., Naumann, E.A., Yang, C.T., Schier, A.F., Freeman, J., Engert, F., and Ahrens, M.B. (2016). Brain-wide mapping of neural activity controlling zebrafish exploratory locomotion. *eLife* *5*, e12741.
47. Chinchor, N. (1992). MUC-4 evaluation metrics. In *Proceedings of the 4th Conference on Message Understanding (Association for Computational Linguistics)*, pp. 22–29.
48. Anderson, D.J., and Perona, P. (2014). Toward a science of computational ethology. *Neuron* *84*, 18–31.
49. Gomez-Marin, A., Paton, J.J., Kampff, A.R., Costa, R.M., and Mainen, Z.F. (2014). Big behavioral data: psychology, ethology and the foundations of neuroscience. *Nat. Neurosci.* *17*, 1455–1462.
50. Krakauer, J.W., Ghazanfar, A.A., Gomez-Marin, A., MacIver, M.A., and Poeppel, D. (2017). Neuroscience needs behavior: correcting a reductionist bias. *Neuron* *93*, 480–490.
51. Bargmann, C.I., and Newsome, W.T. (2014). The Brain Research Through Advancing Innovative Neurotechnologies (BRAIN) initiative and neurology. *JAMA Neurol.* *71*, 675–676.
52. Mott, M.C., Gordon, J.A., and Koroshetz, W.J. (2018). The NIH BRAIN Initiative: advancing neurotechnologies, integrating disciplines. *PLoS Biol.* *16*, e3000066.
53. Dulac, C., Maunsell, J., Anderson, D., Anikeeva, P., Arlotta, P., Churchland, A., Deisseroth, K., Denison, T., Deshler, J., Dzirasa, K., et al. (2019). The Brain Research through Advancing Innovative Neurotechnologies (BRAIN) initiative 2.0. <https://braininitiative.nih.gov/>.
54. Orger, M.B., Kampff, A.R., Severi, K.E., Bollmann, J.H., and Engert, F. (2008). Control of visually guided behavior by distinct populations of spinal projection neurons. *Nat. Neurosci.* *11*, 327–333.
55. Antinucci, P., Figueira, M., and Bianco, I.H. (2019). A pretectal command system controls hunting behaviour. *bioRxiv*. <https://doi.org/10.1101/637215>.
56. Bianco, I.H., and Engert, F. (2015). Visuomotor transformations underlying hunting behavior in zebrafish. *Curr. Biol.* *25*, 831–846.
57. Semmelhack, J.L., Donovan, J.C., Thiele, T.R., Kuehn, E., Laurell, E., and Baier, H. (2014). A dedicated visual pathway for prey detection in larval zebrafish. *eLife* *3*, e04878.
58. Klein, R.M. (2000). Inhibition of return. *Trends Cogn. Sci.* *4*, 138–147.
59. Wee, C.L., Song, E.Y., Johnson, R.E., Ailani, D., Randlett, O., Kim, J.Y., Nikitchenko, M., Bahl, A., Yang, C.T., Ahrens, M.B., et al. (2019). A bidirectional network for appetite control in larval zebrafish. *eLife* *8*, e43775.
60. Muto, A., Lal, P., Ailani, D., Abe, G., Itoh, M., and Kawakami, K. (2017). Activation of the hypothalamic feeding centre upon visual prey detection. *Nat. Commun.* *8*, 15029.
61. Abdelfattah, A.S., Kawashima, T., Singh, A., Novak, O., Liu, H., Shuai, Y., Huang, Y.C., Campagnola, L., Seeman, S.C., Yu, J., et al. (2019). Bright and photostable chemigenetic indicators for extended *in vivo* voltage imaging. *Science* *365*, 699–704.
62. Trivedi, C.A., and Bollmann, J.H. (2013). Visually driven chaining of elementary swim patterns into a goal-directed motor sequence: a virtual reality study of zebrafish prey capture. *Front. Neural Circuits* *7*, 86.
63. Portugues, R., Feierstein, C.E., Engert, F., and Orger, M.B. (2014). Whole-brain activity maps reveal stereotyped, distributed networks for visuomotor behavior. *Neuron* *81*, 1328–1343.
64. Bianco, I.H., Ma, L.H., Schoppik, D., Robson, D.N., Orger, M.B., Beck, J.C., Li, J.M., Schier, A.F., Engert, F., and Baker, R. (2012). The tangential nucleus controls a gravito-inertial vestibulo-ocular reflex. *Curr. Biol.* *22*, 1285–1295.
65. Bolton, A.D., Haesemeyer, M., Jordi, J., Schaechtle, U., Saad, F.A., Mansinghka, V.K., Tenenbaum, J.B., and Engert, F. (2019). Elements of a stochastic 3D prediction engine in larval zebrafish prey capture. *bioRxiv*. <https://doi.org/10.1101/755777>.
66. Harpaz, R., Tkačik, G., and Schneidman, E. (2017). Discrete modes of social information processing predict individual behavior of fish in a group. *Proc. Natl. Acad. Sci. USA* *114*, 10149–10154.
67. Bod'ová, K., Mitchell, G.J., Harpaz, R., Schneidman, E., and Tkačik, G. (2018). Probabilistic models of individual and collective animal behavior. *PLoS ONE* *13*, e0193049.
68. Sharma, A., Johnson, R., Engert, F., and Linderman, S. (2018). Point process latent variable models of larval zebrafish behavior. In *Advances in Neural Information Processing Systems*, pp. 10919–10930.
69. Gelman, A., and Hill, J. (2006). *Data Analysis Using Regression and Multilevel/Hierarchical Models* (Cambridge University Press).
70. Linderman, S.W., Nichols, A.L., Blei, D.M., Zimmer, M., and Paninski, L. (2019). Hierarchical recurrent state space models reveal discrete and continuous dynamics of neural activity in *C. elegans*. *bioRxiv*. <https://doi.org/10.1101/621540>.
71. Kim, D.H., Kim, J., Marques, J.C., Grama, A., Hildebrand, D.G.C., Gu, W., Li, J.M., and Robson, D.N. (2017). Pan-neuronal calcium imaging with cellular resolution in freely swimming zebrafish. *Nat. Methods* *14*, 1107–1114.
72. Cong, L., Wang, Z., Chai, Y., Hang, W., Shang, C., Yang, W., Bai, L., Du, J., Wang, K., and Wen, Q. (2017). Rapid whole brain imaging of neural activity in freely behaving larval zebrafish (*Danio rerio*). *eLife* *6*, e28158.
73. Naumann, E.A., Kampff, A.R., Prober, D.A., Schier, A.F., and Engert, F. (2010). Monitoring neural activity with bioluminescence during natural behavior. *Nat. Neurosci.* *13*, 513–520.
74. Symboulidis, P., Lauri, A., Stefanou, A., Cappetta, M., Schneider, S., Jia, H., Stelzl, A., Koch, M., Perez, C.C., Myklatun, A., et al. (2017). NeuTracker-imaging neurobehavioral dynamics in freely behaving fish. *Nat. Methods* *14*, 1079–1082.
75. Muto, A., Ohkura, M., Abe, G., Nakai, J., and Kawakami, K. (2013). Real-time visualization of neuronal activity during perception. *Curr. Biol.* *23*, 307–311.
76. Markowitz, J.E., Gillis, W.F., Beron, C.C., Neufeld, S.Q., Robertson, K., Bhagat, N.D., Peterson, R.E., Peterson, E., Hyun, M., Linderman, S.W., et al. (2018). The striatum organizes 3d behavior via moment-to-moment action selection. *Cell* *174*, 44–58.e17.
77. Allen, W.E., Chen, M.Z., Pichamoorthy, N., Tien, R.H., Pachitariu, M., Luo, L., and Deisseroth, K. (2019). Thirst regulates motivated behavior through modulation of brainwide neural population dynamics. *Science* *364*, 253.

## STAR★METHODS

### KEY RESOURCES TABLE

REAGENT or RESOURCE	SOURCE	IDENTIFIER
Deposited Data		
Compressed Behavioral Data	This paper	Mendeley Data: <a href="https://dx.doi.org/10.17632/8sb4ywbx7f.1">https://dx.doi.org/10.17632/8sb4ywbx7f.1</a>
Experimental Models: Organisms/Strains		
7-8 days-post-fertilization; <i>Danio rerio</i> : mitfa <sup>-/-</sup> ( <i>nacre</i> )	Harvard University; MCB Fish Facility	N/A
Software and Algorithms		
Statistical Modeling Code	This paper	<a href="https://github.com/slinderman/beast">https://github.com/slinderman/beast</a>

### LEAD CONTACT AND MATERIALS AVAILABILITY

Further information and requests for resources should be directed to and will be fulfilled by the Lead Contact, Robert Evan Johnson ([robertevanjohnson@gmail.com](mailto:robertevanjohnson@gmail.com)). This study did not generate new unique reagents.

### EXPERIMENTAL MODEL AND SUBJECT DETAILS

All fish were 7-8 days post-fertilization (dpf) mitfa<sup>-/-</sup> (*nacre*) zebrafish raised at ~27°C. Fish were given abundant live paramecia as food beginning at 5 dpf. On test day, fish from the *fed* group remained in their Petri dish with abundant paramecia while fish from the *starved* group were placed in clean water for ~2.5-5 h prior to testing. Testing was performed between 10 AM and 6 PM with 4-6 fish usually tested per day. All protocols and procedures were approved by the Harvard University/Faculty of Arts and Sciences Standing Committee on the Use of Animals in Research and Teaching (Institutional Animal Care and Use Committee).

### METHOD DETAILS

#### BEAST Design

The gantry was acquired from CNC Router Parts (CRP4848 4ft x 4ft CNC Router Kit; <http://www.cncrouterparts.com/>) and was modified to run upside-down on top of a support structure constructed from aluminum T-slotted framing available through 80/20 (<http://www.8020.net/>). Three electric brushless servo motors (CPM-MCPV-3432P-ELN ClearPath Integrated Servo Motors) and 3 Amp DC Power Supply (E3PS12-75) were acquired from Teknic (<https://www.teknic.com/>). The camera (EoSens 3CL) was acquired from Mikrotrotron (<https://mikrotrotron.de/>) with a frame-grabber from National Instruments (NI PCIe-1433; <http://www.ni.com/>). The camera lens was acquired from Nikon (AF-S VR Micro-Nikkor 105mm f/2.8G IF-ED; <https://www.nikonusa.com/en/index.page>). A long-pass infrared filter was placed over the lens (62 mm Hoya R72; <https://hoyafilter.com/>) to block light from the projector and collect transmitted light from an array of 16 IR-LED security dome lights (850 nm Wide Angle Dome Illuminators) positioned on the air table below the fish tank. The projector was acquired from Optoma (Optoma GT1080; <https://www.optoma.com/>) and mounted on the side of the air table to project onto a diffusive screen (Rosco Cinegel 3026 Tough White Diffusion (216); <https://www.stagelightingstore.com/>) embedded in the bottom of the plexiglass tank.

#### Data Acquisition

The walls of the observation arena were assembled with light gray LEGO blocks to confine the fish to a water volume of 300 × 300 × 4 mm. Approximately 15 mL of water containing a high density of live paramecia were added near the center of the arena prior to testing each fish. This paramecia stock also contained some rotifers and algae particles. For testing, single fish were transferred to the arena where inwardly drifting concentric gratings were projected to bring the fish to the arena center. Zebrafish larvae tend to turn and swim in the direction of perceived whole-field motion, a reflexive behavior called the optomotor response, and we leverage this response to relocate the fish. Once the overhead camera detected the arrival of the fish, the first observational trial was initiated and the drifting gratings were replaced by a static color image of small pebbles, a natural image with reasonably high spatial contrast. Next, the camera moved automatically on the gantry to maintain position above the fish and capture video with a frame-rate of 60Hz and 2 ms exposure duration per frame. The fish was tracked for 3 min or until it reached the edge of the arena or tracking failed. The fish could evade the tracking camera with a high-speed escape maneuver, but these events were fairly rare. At the end of each trial, the camera returned to the arena center, video data was transferred from memory to hard disk, and concentric gratings were once again used to bring the fish back to the arena center to initiate another trial (up to 18 trials per fish). If the fish did not return to the center within 10-15 min, the experiment was terminated. The tracking algorithm was written to keep the darkest pixel in the image (usually contained within one of the eyes of the fish) within a small bounding

box located at the image center. If the darkest pixel was located outside this bounding box, a command was sent to the motors to reposition the camera to the location of that darkest pixel. In this way, the camera moved smoothly from point to point to follow the fish, using the “Pulse Burst Positioning Mode” setting for the ClearPath motors. We run the ClearPath motors with Teknic’s jerk-limiting RAS technology engaged to generate smooth motion trajectories and minimize vibration during point to point movement. Experiments were run using PsychToolBox in MATLAB.

### Statistical Models

See [Methods S1](#) for statistical modeling details.

## QUANTIFICATION AND STATISTICAL ANALYSIS

### Image Registration and Fish Pose Estimation

In every image frame, connected component pixel regions corresponding to the left eye, right eye, and swim bladder were identified. The fish head center was defined as the average position of the centers of these 3 regions of interest. Heading direction is defined as the direction of the vector from the swim bladder center to the midpoint between the two eye centers. This information is used to translate and rotate each image for subsequent pose estimation and environment analysis. Only image frames in which all postural features could be extracted were included for further analysis. One common issue with pose estimation was caused by body roll of the fish, usually during an attempt to strike at a prey object, in which the fish would roll (rotate around its rostral-caudal axis) enough for one eye to occlude the other from the view of the overhead camera. Rather than estimate eye vergence angles in these situations, these image frames were excluded. Another common issue was caused by high-speed maneuvers by the fish during which a 2 ms exposure was insufficient to capture a suitably sharp image, thus causing either image registration or pose estimation algorithms to be compromised. We included only image frames in which all postural features could be accurately extracted for further analysis. Video segments containing problematic frames were split into separate video segments.

### Temporal Segmentation of Bout and Interbout Epochs

Bout and interbout epochs were identified by taking the absolute value of the frame to frame difference in heading angle and thresholding this time-series at 0.7 degrees. This binary signal was then dilated (radius = 2 elements) and eroded (radius = 1 element) with built-in MATLAB functions (`imdilate`, `imerode`) to merge bout fragments and expand bout epochs to include one extra frame at the beginning and end of each bout. These operations set the minimal duration of both bout and interbout epochs to 3 frames (50 ms).

### Bout Summary Statistics

$\Delta$ heading per bout: The change in heading angle per bout was calculated by averaging the heading direction of the fish over all frames in the preceding interbout epoch and subtracting this value from the average heading direction through all frames in the following interbout epoch. Positive values are assigned to leftward bouts.

$|\Delta$ heading| per bout: The absolute value of  $\Delta$ heading per bout.

distance traveled per bout: The change in head position per bout was calculated by averaging the position of the fish head in the arena over all frames in the preceding interbout epoch (starting position) and also for the frames in the following interbout epoch (ending position). The distance between these two points is the distance traveled per bout.

$|\Delta$ tail-shape| per bout: This non-negative 1-dimensional quantity summarizes how much the tail changes shape during the 10 frames used to represent each swim bout (as in [Figure 2A](#)). To compute this quantity, let the 10-frame tail angle measurements be placed in an array  $T$  with shape  $20 \times 10$ . First, the magnitude of frame to frame changes in each tail segment angle are computed to give a new array with shape  $20 \times 9$ .  $|\Delta$ tail-shape| is the sum of the absolute values of these 180 array elements. This value is divided by 180 to give units: radians per segment per frame. In MATLAB syntax, this is computed as:

$$\text{abs\_delta\_tail\_shape} = \text{sum}(\text{sum}(\text{abs}(\text{diff}(T, n = 1, \text{dim} = 2))))/180$$

Several additional summary statistics are used to describe the fish eyes during each bout. These metrics are computed from the 10-frame representations of each bout and are further described in [Figure S3](#).

### tSNE Input

Each swim bout is represented as a 220-dimensional vector encoding the posture of the fish through 10 image frames beginning at bout initiation with 20 tail vectors and 2 eye vergence angles per frame (see also [Figure S1](#)). All rightward bouts ( $\Delta$ heading < 0) were mirror reflected prior to running tSNE by swapping the left and right eye measurements and multiplying all tail angle measurements by  $-1$ . Because tail measurements are tenfold more abundant than eye measurements and we sought to emphasize eye data in our clustering, we decreased the relative magnitude of the tail measurements by encoding tail measurements in radians and encoding eye measurements in degrees. In practice, we found that we could identify roughly the same bout-classes across a fairly wide range

of scaling factors used to emphasize eye measurements relative to tail measurements. While it is common to preprocess data with PCA prior to running tSNE, we achieved qualitatively similar embedding results with and without this step, so we simply ran tSNE on the 220-D inputs.

Each of the 200,559 swim bouts are represented as 220-D vectors as described above and are embedded in a 2-D space with tSNE. We implement tSNE with Barnes-Hut approximations with CUDA to decrease tSNE runtime ([https://github.com/georgedimitriadis/t\\_sne\\_bhcuda](https://github.com/georgedimitriadis/t_sne_bhcuda)). Euclidean distance was used as a distance metric. Following embedding, 5 bout classes were identified with the routines described in Figure S2. The 3 largest clusters were then further subdivided by kinematic variables,  $|\Delta\text{heading}|$  and  $|\Delta\text{tail-shape}|$ , as described in Figure S2 and above.

### Identifying and Encoding Environmental Information

Objects near the water surface preceding each swim bout are identified with image processing routines. The focal plane of our camera was positioned near the water surface, so objects near the water surface are in focus while objects near the tank bottom are blurry. We therefore wrote routines to isolate high spatial contrast objects. Following image translation and rotation, a stack of the 6 images preceding bout initiation are cropped as in Figure 1J. High spatial contrast objects are identified in MATLAB by filtering each image in this stack with a Laplacian of Gaussian 2-D filter (size =  $13 \times 13$  pixels, sigma = 1.6). Contiguous 3-D object volumes in this image stack are smoothed with 3-D dilation and erosion. The average position of each object in the image frame preceding bout initiation was used to encode object location with the extrinsic feature  $\mathbf{v}_{loc}$ . The number of pixels assigned to each object in this final frame was used to encode object size with the extrinsic feature  $\mathbf{v}_{size}$ . The velocity of each object was computed by calculating the distance between the center of mass of each object in the 6<sup>th</sup> image frame preceding bout initiation (t-minus 100 ms) and the 1<sup>st</sup> frame preceding bout initiation (t-minus 17 ms) and dividing by the time elapsed. If an object was not properly segmented through all 6 frames, the velocity was calculated from fewer frames (with a minimum of 3 frames). The velocity vectors for each object were used to encode x-velocity and y-velocity in the extrinsic features  $\mathbf{v}_x$  and  $\mathbf{v}_y$ . While the image resolution is sufficient to extract additional features such as the orientation, eccentricity, and detailed shape of each object, we have not yet included this information in our predictive models.

### Intrinsic Features to Predict Interbout Intervals and Bout-types

*preceding interbout interval*: the duration of the preceding interbout interval in seconds. For models to predict interbout interval duration ( $i_n$ ), this is the duration of interbout  $i_{n-1}$ . For models to predict bout-type ( $\mathbf{b}_n$ ), this is the duration of interbout  $i_n$ .

*preceding bout-type*: the category (i.e., bout-type) of the preceding swim bout. There are 18 bout-types, each of which is composed of left and right versions, giving 36 categories in total.

*hunt dwell-time*: the integer number of observed preceding consecutive hunting bouts (i.e., *J-turn*, *pursuit*, *abort*, *strike*). As hunt sequences extend, this value increases.

*explore dwell-time*: the integer number of observed preceding consecutive exploring bouts. For all predicted interbout intervals and bout-types, either *hunt dwell-time* or *explore dwell-time* will be zero, with the other being a positive integer. Only the contiguous bout sequence containing the predicted interbout interval ( $i_n$ ) or bout-type ( $\mathbf{b}_n$ ) is used to define these feature values.

*tank-time*: the amount of time (in minutes) elapsed since the first trial was initiated for that fish.

### Extrinsic Features to Predict Bout-types

$\mathbf{v}_{loc}$ : locations of potential prey in the local environment.

$\mathbf{v}_{size}$ : sizes of potential prey in the local environment.

$\mathbf{v}_x$ : relative x-velocities of potential prey in the local environment.

$\mathbf{v}_y$ : relative y-velocities of potential prey in the local environment.

See Figure S4 for more information on intrinsic and extrinsic feature encoding.

### Simulations

For our *combo renewal process* simulations, we simulated an environment with prey objects that move as biased random walking particles. Each particle has a constant size and speed. These particles influence bout-type selection as their locations, sizes, and relative velocities are encoded with the extrinsic features  $\mathbf{v}_{loc}$ ,  $\mathbf{v}_{size}$ ,  $\mathbf{v}_x$ , and  $\mathbf{v}_y$ . We simulated 50 *fed* and 50 *starved* fish for 40 min each (in 20 two-minute trials). Similar to our real experiments, prey are distributed with a centro-peripheral gradient, with the highest density of prey located near where trials begin. To simulate a behavioral sequence, an interbout interval duration is selected by randomly sampling from an interbout interval distribution generated from the *combo* interbout interval model. Next, a bout-type is selected by randomly sampling from a bout-type probability distribution generated from the *combo* bout model. Upon selection of a bout-type, we move the fish through its virtual world along the bout-type specific trajectories described in Figure S7. Since the *combo* bout model depends on the environment in addition to behavioral history and hunger state, the virtual prey objects influence the fish's behavioral trajectory. We call this combined bout and interbout model a *combo renewal process*. For comparison, we simulate 50 *fed* and 50 *starved* fish with a simpler model in which interbout intervals and bout-types depend only on *preceding bout-type* ( $\mathbf{b}_{n-1}$ ). In these simulations, interbout interval durations are sampled from a probability distribution generated by the selected form of the *preceding bout-type* feature (*split- $\mathbf{b}_{n-1}$* ), and bout-types are sampled from a bout-type probability distribution generated from the selected form of the *preceding*

*bout-type* feature (*pooled- $\mathbf{b}_{n-1}$* ). This model is referred to as a *first-order Markov renewal process*, and has no environmental dependencies. For both the *combo renewal process* simulations and the *first-order Markov renewal process* simulations, model weights are set at the maximum *a posteriori* (MAP) estimate of the GLM weights from the trained models.

#### **DATA AND CODE AVAILABILITY**

Compressed behavioral data (Mendeley: <https://dx.doi.org/10.17632/8sb4ywbx7f.1>) and statistical models (<https://github.com/slinderman/beast>) are available online. Uncompressed data available upon request.